Islamic Azad University

Journal of

Optoelectronical Nanostructures

Winter ۲۰۲۱ / Vol. ٦, No. ۱

Research Paper

Host Liquid Effect on Thermo-Optical Pattern of a Self-Phase Modulated Laser Beam Passing Through Au Nanoparticles Colloids

Hoda Aleali [۱*], Ahmad Mehramiz[۲], Elham Valizadeh Pilehroud[۲]

[۱] Department of metrology, Research Center of Quality Assessment and Management Systems, Standard Research Institute (SRI), Karaj, ۳۱۷٤۷۳٤٥٦۳, Iran

[۲] Department of Physics, Faculty of Basic Sciences, Imam Khomeini International University, Qazvin, Iran

Received:
Revised:
Accepted:
Published:

Use your device to scan and read the article online

DOI:

Keywords:
thermo-optical nonlinearity, host liquid's properties, far-field intensity, colloidal gold nanoparticles,

Abstract

In this paper, the influence of host liquid's properties on far-field intensity distribution of a continuous Gaussian laser beam passing through the synthesized colloidal gold nanoparticles (AuNPs) is experimentally and numerically studied considering the different form of heat transfer modes. Our results reveal that dispersed NPs in liquids with more viscosity or less thermal expansion coefficient, lead to more concentric far-field diffraction patterns. By changing the viscosity and thermal expansion coefficient, the form of diffraction patterns due to the convection effect, can dramatically change compared to the strength of the thermal nonlinear refraction. The effect of the linear absorption coefficient of the medium on diffraction patterns of the colloids is also investigated. It is shown that by increasing the linear absorption coefficient of the medium, the number of the rings and the beam divergence increase under exposure of the ٥۳۲ nm laser beam. Our observations show the excellent sensitivity of the diffraction ring pattern technique to characterize the

Citation: Hoda Aleali, A. Mehramiz, E. Valizadeh Pilehroud. Host Liquid Effect on Thermo-Optical Pattern of a Self-Phase Modulated Laser Beam Passing Through Au Nanoparticles Colloids. **Journal of Optoelectronical Nanostructures.** ۲۰۲۰; ۱ (۱): ٤۸_٥۸

***Corresponding author:** Hoda Aleali
Address: Department of metrology, Standard Research Institute (SRI), Karaj, ۳۱۷٤۷۳٤٥٦۳, Iran. **Tell:** ۰۰۹۸۹۱٦۳۳۲٥٤٥٦ **Email:** Hoda Aleali @gmail.com

self-phase modulation, photonic devices.

different modes of heat transfer and thermo-optical nonlinear properties of the NPs colloids.

١. INTRODUCTION

Linear and nonlinear optical properties of nanomaterials have attracted many attentions resulting in optimal designing of optical devices [١-٦]. Among the nanomaterials, gold nanoparticles have been introduced based on their optical properties as a suitable candidate for applications such as optical hyperthermia, new generation of medical devices, the resonance of the surface plasmon (SPR)-based optical biosensor, optical devices, etc. [٦-٩]. AuNPs colloids are able to absorb laser beam energy due to their excitation of surface plasmon resonance [١٠-١٩]. In this case, after absorption of the laser beam, the colloids are locally heated, and the temperature of the heated region increases, causing laser induced thermal lens effect. Great attention has been paid to study the thermal nonlinear properties of the colloidal nanoparticles under exposure to CW laser light at wavelength of ٥٣٢ nm using the Z-scan method [١٠-١٨]. It has been found that thermal third-order nonlinear refractive index induced by linear absorption of laser energy is the main mechanism responsible for observed nonlinearity in the colloids.

Different refractive indexes originated by thermal third-order nonlinear refraction result in a phase shift of light wave that creates an interference pattern at a far-field distance. Recently, the far-field intensity distribution of the Gaussian laser beam passing through the liquids has been presented experimentally and theoretically for optical photonic devices [٢٠-٣٠]. Karimzadeh [٢٦] has shown the temporal evolution of the diffraction patterns formed on a screen because of conduction and convection effects. At first, a bright spot is created. Then, the size of spot quickly increases and interference rings are appeared. For several seconds, a flattening of the top is obtained and considerably transformed into stable rings. The observed time development could be due to the following mechanisms: First, the thermal conduction self-phase modulation occurred in the medium; this creates the interference rings. Second, the top flattening of rings appears due to the thermal convection effects. Shi, et al. have shown that the distorted diffraction ring pattern affects the spatial self-phase modulation applications in nonlinear photonic devices such as the all-optical switch and all-optical information converter that can fairly tune the response time [٣١]. One can find that changing the surrounding solvent and concentration of colloidal metal NPs can change the properties of colloids such as absorption spectrum, optical limiting and nonlinear optical properties [٣٢-٣٥]. In order to search for nanomaterials that meet the requirement of implementing proper optical devices, it would be necessary to predict their behavior under exposure to laser light.

To this aim, the far-field intensity distribution of the CW laser beam passing through the NPs colloids with different host medium as a thermal nonlinear medium, including thermal conduction and thermal convection in the heat transfer equation, is numerically analyzed. Using the thermal nonlinear coefficient of the colloids extracted by Z-scan method, the influence of the physical properties of the host medium on intensity profile at a far distance is predicted. The obtained numerical far-field intensity distribution of the CW laser beam passing through the AuNP colloids are confirmed by the experimental results using ٥٣٢ nm laser beam. Finally, the key physical mechanism that contributes to the strongest thermo-optical effect of the colloids with the lowest thermal conductivity is described.

٢. Numerical studies of the pattern of self-phase modulated laser

٢،١. The laser interaction with the thermal nonlinear medium

In order to analyze the far-field intensity distribution of the laser beam passing through the thermal nonlinear medium, the electric field at any position z of the sample must be calculated. At first, we need to solve the Maxwell equations for the interaction of the laser beam and the nonlinear sample. Then, the propagation of the laser beam in the free space from the exit surface of the sample to the observation plane at a far distance is calculated. The magnitude and phase of the electric field of a Gaussian beam change in the z direction due to passing through the nonlinear thin media. One can calculate the phase shift, Δφ, and the electric field intensity, I, as follows [٣٦-٣٧]:

$$\frac{d\Delta\varphi}{dz} = \frac{٢\pi}{\lambda}\Delta n(I) \qquad (١)$$

$$\frac{dI}{dz} = -\alpha(I)I \qquad (٢)$$

where z is the propagation length inside the sample, α(I) is the absorption coefficient, including linear and nonlinear absorption, and Δn(I) is the variation of the sample refractive index. It is assumed that the third-order nonlinear refraction is the only mechanism for generating nonlinear effects, and nonlinear absorption phenomena are negligible in the sample. Then, the refractive index and the material absorption coefficient are written as $\Delta n(I) = n_{٠} + n_{٢}I$ and $\alpha(I) = \alpha_{٠}$, respectively, where $n_{٠}$ is the linear refractive index, $n_{٢}$ is the third-order nonlinear refractive index, and $\alpha_{٠}$ is the linear absorption coefficient.

When the sample is exposed to laser light, it absorbs a portion of light energy. The absorbed energy creates a spatial temperature distribution in the sample, followed by the process of heat diffusion in the medium. The created temperature gradient acts as a lens, and a phase difference in the wave occurs that is called the thermal lens effect [١٠-١١, ٣٠, ٣٨-٤٣]. This effect produces a diffraction pattern on the far-field plane. The intensity of the diffracted laser beam can be obtained at a distant screen perpendicular to the direction of light propagation, using the Fraunhofer approximation in the Fresnel-Kirchhoff diffraction integral as:

$$I(x',y',t) = \left| E.(t)\frac{i\pi\omega^{2}}{\lambda d}\exp(ikd)\exp\left(-\frac{\alpha.L}{2}\right)\times\int_{-\infty}^{\infty}dx\int_{-\infty}^{\infty}dy\exp\left(-\frac{x^{2}+y^{2}}{\omega^{2}}\right)\right.$$

$$\left.\times\exp\left(-i\left[k\frac{x^{2}+y^{2}}{2R}-\Delta\phi(x,y,t)\right]\right)\times\exp\left(-ik\frac{xx'+yy'}{d}\right)\right|^{2} \qquad (٣)$$

where ω is the beam radius, λ is the laser beam wavelength in vacuum, $k = 2\pi/\lambda$ is the wavenumber, R is the radius of curvature of the beam wave front, d is the distance between the sample and the screen in the far-field, L is the effective length of the sample, and $E.(t)$ is the electric field at the focal point. By determining the thermo-optical phase shift of the light electric field due to heat transfer in the sample, the far-field intensity distribution of the Gaussian laser beam on the observation plane (equation ٣) can be solved numerically.

٢,٢. Thermo-optical phase shift

To obtain the thermo-optical phase shift, first, we need to solve the heat transfer equation to obtain the temperature distribution along with the laser beam propagation. Heat transfer is a process whereby thermal energy is transferred in response to a temperature difference by various mechanisms, such as thermal conduction and thermal convection. In the case of convection, when the light radiation absorbs the energy, the temperature of the irradiated region increases, decreasing its density. In this case, the gravitational force applied to the particles causes the higher-density particles in the upper part of the radiation to move downwards and replaces the lower-density particles. Therefore, a convective flow is created in the liquid. Given two modes of heat transfer, including conduction and convection, the heat transfer equation can be formulated as follows:

$$C_p\rho\left(\frac{\partial}{\partial t}[\Delta T(x,y,t)] + v_x\frac{\partial[\Delta T(x,y,t)]}{\partial x}\right) - K\nabla^{2}[\Delta T(x,y,t)] = \alpha I(x,y) \quad (٤)$$

Where $C_p$is the specific heat capacity, ρ is the density, K is the thermal conductivity coefficient, $v_x = \beta g \Delta T_m \pi \omega_0^2 / 16 \mu$ is the convective velocity due to the equilibrium between the fluid viscous forces and the heat buoyancy force and directed [20, 31], β is the thermal expansion of the coefficient, ΔT_m is the maximum temperature, g is the gravitational acceleration, ω_0 is the laser beam waist, and μ is the viscosity of the sample. By applying the proper boundary conditions [38-39] and the Green's function for the convection and conduction heat transfer equation [40], the temperature distribution can be obtained in terms of the absorbed energy of the laser at each point *x* and *y* after the time t [25, 30].

$$\Delta T(x,y,t) = \frac{\alpha P}{\pi C_p \rho}\left\{\int_0^t \frac{d\tau}{8D\tau+\omega^2}\exp\left(-\frac{2[(x-v_x\tau)^2+y^2]}{8D\tau+\omega^2}\right)\right\} \quad (5)$$

where $D = K/C_p\rho$ is the heat diffusion coefficient. The induced temperature gradient changes the refractive index of the material according to relation $n(x,y,t) = n_0 + dn/dT\,\Delta T(x,y,t)$, where dn/dT is the thermo-optical coefficient of the sample. Created phase difference due to the change in refractive index is obtained by substituting equation 5 in relation $\Delta\phi(x,y,t) = 2\pi/\lambda\, L[n(x,y,t)-n(0,0,t)]$ as follows [25]:

$$\Delta\phi(x,y,t) = 2\theta D\int_0^t \frac{d\tau}{8D\tau+\omega^2}\left\{\exp\left(-\frac{2[(x-v_x\tau)^2+y^2]}{8D\tau+\omega^2}\right) - \exp\left(-\frac{2(v_x\tau)^2}{8D\tau+\omega^2}\right)\right\} \quad (6)$$

where $\theta = dn/dT\,\alpha P L/\lambda K$ is the on-axis phase shift.

The numerically far-field intensity distribution of the Gaussian laser beam passing through the thermal nonlinear media with different viscosities and thermal expansion coefficients are shown in Fig. 1. In this study, the input parameters were set based on reliable and real amounts [25]. For this simulation, $\mu_1 = 1.36 \times 10^{-6}\,s^{-1}m^2$, $\beta_1 = 750 \times 10^{-6}\,k^{-1}$ and the on-axis phase shift is taken with an arbitrary magnitude of $\theta \cong 70.8$. According to the recently reported values of the linear absorption coefficient of different colloidal nanoparticles with the radius range of 10-70 nm, this parameter is arbitrarily set as $\alpha_0 = 0.5\ cm^{-1}$[10-11, 25, 42-43]. The thermal diffusivity is also fixed at $D = 0.88 \times 10^{-7}\,s^{-1}m^2$.

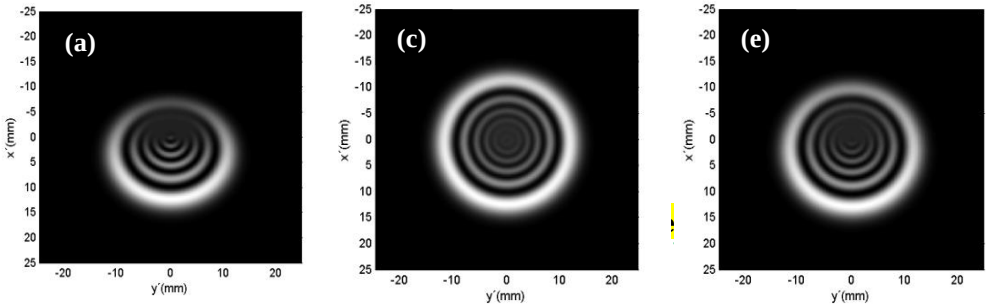

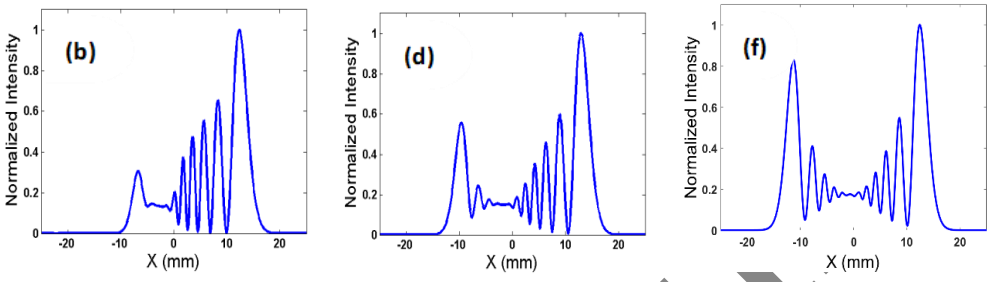

Fig. ١. The simulated far-field diffraction patterns and normalized intensity of the laser beam propagating through the colloidal nanoparticles with host medium viscosities of a, b) $\mu = \mu_{\circ}$; c, d) $\mu = ٢\mu_{\circ}$; e, f) $\mu = ٦\mu_{\circ}$ and with thermal expansion coefficients of a, b) $\beta = \beta_{\circ}$; c, d) $\beta = \beta_{\circ}/٢$; e, f) $\beta = \beta_{\circ}/٦$. It is noted the increasing μ and decreasing β show the same results.

As it is clearly shown in Fig. ١, by increasing the viscosity of the host medium, which causes the convection current to decrease, the diffraction rings pattern and normalized intensity profile become more symmetrical. The results suggest that the convection heat flow can explain the observed asymmetric nature of the far-field intensity distribution in the medium with the lower viscosity. The normalized intensity profiles as a function of *x* are also plotted for the colloids with different viscosity of host medium in Fig. ١(b), ١(d) and ١(f). Compared to the condition of more convective mode, in the less convective mode, the graph is more symmetric with respect to the y-axis (x = ٠). Fig. ١ also shows that by decreasing the thermal expansion coefficient of the host medium, the diffraction rings and normalized intensity profile become more symmetrical due to the decrease in the convection current. As it is clear, by decreasing the thermal expansion coefficient, less particles collide with each other, and less convection occurs. According to Fig. ١, one can find that the obtained number of diffraction rings (about ٦ interference fringes) and beam divergence (about ١٥ mm) are the same for all viscosities and thermal expansion coefficients. It is worth noting that compared to the drastic change in the symmetry of the diffraction pattern arising from a change in convection velocity of the colloids (Fig. ١), the amount of phase shift occurred in the medium does not dramatically change.

The influence of the linear absorption coefficient of the medium on intensity profile at a far distance is also investigated numerically. Fig. ٢ illustrates that by

increasing the linear absorption coefficient, the beam divergence and the number of circular rings increase leading to the significant enhancement of thermal nonlinear effect attributed to either higher linear absorption coefficient of the host medium or higher nanoparticle concentration.

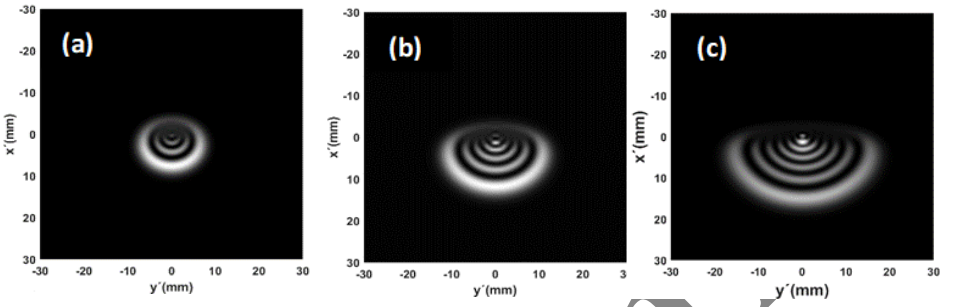

Fig. ٢. The simulated far-field diffraction patterns of the laser beam propagating through the colloidal nanoparticles with linear absorption coefficients of a) $\alpha = \alpha_1 = ٠,٢٥\ cm^{-1}$ b) $\alpha = ٢\alpha_1$ and c) $\alpha = ٤\alpha_1$.

٣. Experimental results and discussion

The diffraction patterns were recorded by a digital camera on a screen in the far field plane about ٤m from the sample using a continuous low power (١٠٠mW) diode-pumped Nd:YVO٤ laser operating at a wavelength of ٥٣٢nm. The Schematic diagram of optical geometry used to record the thermo-optical diffraction patterns for the AuNP colloids is shown in Fig. ٣. In the experimental setup, a continuous laser beam was focused onto the surface of the colloidal gold nanoparticles placed inside a ٥-mm cell by a lens of focal length ٥٠٠ mm. The cell was placed between the lens and the focus point. The spot size in the focal region is ٣٩ mm ($HW^{١}/e^{٢}M$).

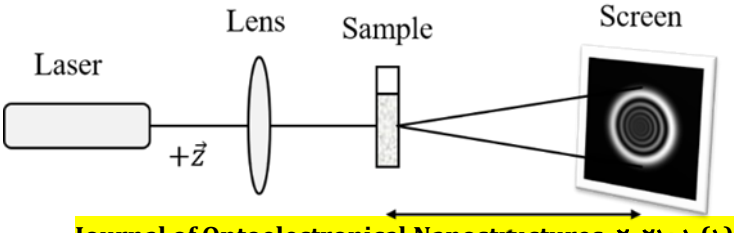

Fig. ٣. Schematic diagram of optical geometry for recording diffraction patterns of the AuNP colloids.

The linear absorption coefficient of about ٠،٥٦ $cm^{-١}$ was set for all samples by dilution of the prepared AuNPs colloids [١١]. To obtain the third-order thermo-optical coefficient of the AuNPs colloids, the closed Z-scan technique has been used (Experimental Z-scan data and the theoretical fits of the colloids have been presented in supplementary material) [١١]. In order to accurately show the effect of host liquid's properties, experiments were performed under the same experimental conditions such as laboratory temperature, experimental geometry, the beam profile, laser intensity and the linear absorption coefficient of the solutions. The experimental patterns of the far-field intensity distribution of continuous laser beam passing through gold nanoparticles in cyclohexanone [١٤], castor oil and water with different optical properties (Table I) are shown in Fig. ٤.

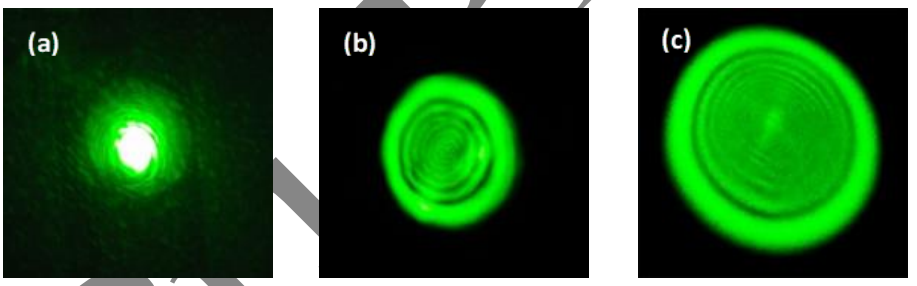

Fig. ٤. The experimental far-field diffraction patterns of the laser beam propagating through the dispersed AuNPs in a) water b) castor oil and c) the reported far-field diffraction patterns of the laser beam propagating through the dispersed AuNPs in cyclohexanone [١٤]. The horizontal axis is y-axis ranging from - ٣٥ mm to ٣٥ mm.

Table I

PHYSICAL PARAMETERS USED FOR SIMULATION OF THE FAR-FIELD INTENSITY DISTRIBUTION OF LASER BEAM PROPAGATION THROUGH GOLD NANOPARTICLE COLLOIDS.

Physical parameters	Water	Castor oil	cyclohexanone
$\rho(kgm^{-٣})$	٩٩٧	٩٥٦	٩٤٧

$c_P(Jkg^{-1}K^{-1})$	٤١٨٦	١٨٠٠	١٩٢٦
$K\ (Wm^{-1}K^{-1})$	٠,٦	٠,١٧	٠,١٣٨
$\beta\ (K^{-1})$	٣٠×١٠^{-٥}	٧٠×١٠^{-٥}	١٢١×١٠^{-٥}
$\mu\ (m^{٢}S^{-1})$	١.٠×١٠^{-٦}	٣.٢×١٠^{-٦}	١.٢٥٨×١٠^{-٦}
$\alpha\ (m^{-1})$	٥٦	٥٧	٥٦
dn/dt (K^{-1})	$٠,٥ \times ١٠^{-٤}$	$١,٨ \times ١٠^{-٤}$	$٢,٣ \times ١٠^{-٤}$

In order to investigate the effect of the linear absorption coefficient that contributes to the thermo-optical properties of the colloids, samples A and B were also synthesized by laser ablation of the pure gold plate in castor oil, with the value of ٠,٢١ and ٠,٨٠ cm^{-1} for α, as described in our previous work [١٣]. Fig. ٥ (a-c) show the diffraction pattern images at applied incident laser power of ٤٠ mW for the colloids at different linear absorption coefficient and pure castor oil.

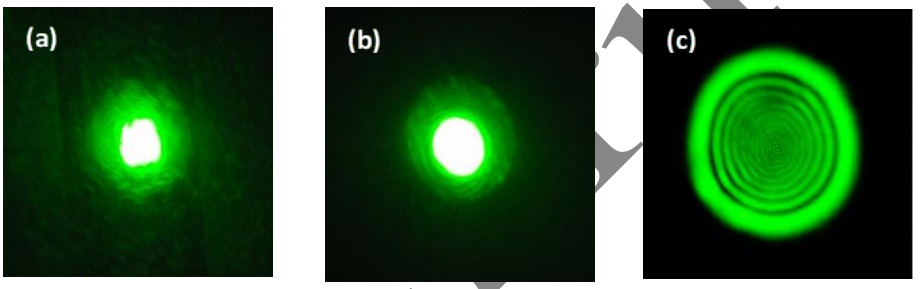

Fig. ٥. The experimental patterns of the laser beam propagating through a) castor oil, b) sample A and c) sample B. The horizontal axis is y-axis ranging from - ٣٥ mm to ٣٥ mm.

We will compare the prediction of the model to the experimental data considering the values of the host medium physical parameters listed in Tables I and II. Fig. ٦ depicts the simulated far-field diffraction patterns of ٦٠ mW applied laser beam propagating through the AuNPs dispersed in water, castor oil and cyclohexanone. As it is clearly illustrated in Fig. ٤ and ٦, the behavior of the experimental results for the diffraction pattern images for the AuNPs colloids are in a good agreement with the prediction of the model. A low divergence of the transmitted laser light is observed without any interference rings in Fig. ٤(a) and ٦(a) for the AuNPs dispersed in water with the highest thermal conductivity. As shown in both Fig. ٤ and ٦, it seems that less symmetrical diffraction pattern for the AuNPs in cyclohexanone is obtained from the highest convection current due to the least viscosity and highest thermal expansion coefficient. Moreover, based on the obtained results, it is obvious that compared to the AuNPs in the castor oil and water, AuNPs in cyclohexanone, with the lowest thermal conductivity,

present the largest far-field diffraction pattern (beam divergence) with more interference fringes. According to the results of the experimental and theoretical data for the closed Z-scan measurement of the AuNPs colloids shown in the supplementary, one can find that unlike the closed Z-scan method, the modes of heat transfer, including conduction and convection can be analyzed and distinguished by the recorded diffraction pattern images for the AuNPs colloids. Thus, this technique can be used to characterize the modes of heat transfer and the thermo-optical properties of nanoparticle colloids.

Table II

PHYSICAL PARAMETERS USED FOR SIMULATION OF THE FAR-FIELD INTENSITY DISTRIBUTION OF LASER BEAM PROPAGATION THROUGH THE SAMPLES A AND B.

Physical parameters	Castor oil	Sample A	Sample B
$\alpha\ (m^{-1})$	٩	٢٠	٧٨
dn/dt (K^{-1})	$١,٤ \times ١٠^{-٤}$	$١,٣ \times ١٠^{-٤}$	$١,٩ \times ١٠^{-٤}$

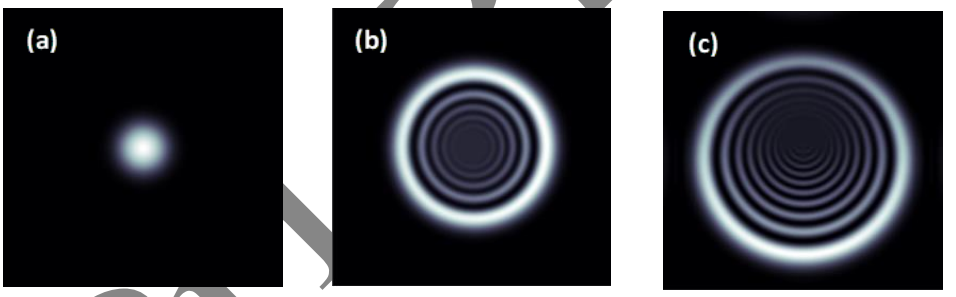

Fig. ٦ The simulated far-field diffraction patterns of the laser beam propagating through the dispersed AuNPs in a) water b) castor oil and c) cyclohexanone. The horizontal axis is y-axis ranging from - ٣٠ mm to ٣٠ mm.

It is clear that the behavior of experimental far-field diffraction patterns shown in Fig. ٥ also confirms the obtained numerical far-field diffraction patterns (Fig. ٧) of the laser beam passing through the AuNPs colloids. Our results show that gold NPs dispersed in the castor oil are able to strongly absorb the wavelength of ٥٣٢ nm light leading to an exhibition of strong thermal nonlinear refractive index of the colloids. It worth mentioning that by increasing the linear absorption coefficient of the colloids, induced nonlinear refractive index enhances which is attributed to the concentration of AuNPs in this work.

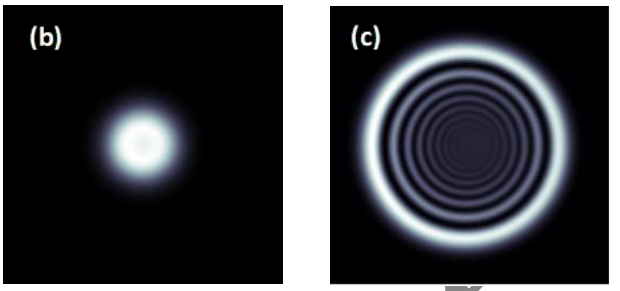

Fig. ۷. The simulated far-field diffraction of the laser beam propagating through a) castor oil, b) sample A and c) sample B, respectively. The horizontal axis is y-axis ranging from -۳۰mm to ۳۰mm.

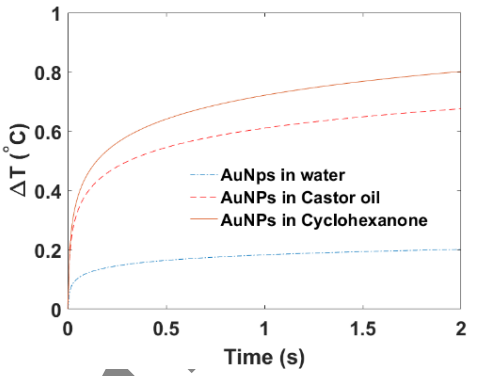

Fig. ۸. The time development of the temperature changes during laser beam propagating through AuNPs in different liquid environments, including water, castor oil, and cyclohexanone.

In order to investigate the key physical mechanism that contributes to the strong thermo-optical effect of the AuNP colloids, the amount of temperature difference in the center of the laser beam along with the z-axis is estimated. Fig. ۸ shows the time development of the temperature changes during laser beam propagation in AuNPs in different liquid environments, including water, castor oil, and cyclohexanone using equation ۵. As it is shown in this figure, at the applied low power laser irradiation, the temperature increases over time development of heat transfer. After the time t, the temperature reaches a maximum then remains clamped at a constant value. Our results in this Fig. show that the maximum temperature difference induced in the center of the laser beam passing through the liquid with the lowest thermal conductivity is the highest and leads to the largest thermal nonlinear refraction.

٤. CONCLUSION

The far-field intensity distribution of a continuous Gaussian laser beam passing through the gold nanoparticles suspended in liquids with different physical properties was numerically and experimentally investigated to characterize the heat transfer and thermo-optical properties. We found that by increasing the thermal expansion coefficient, the top of the diffraction ring pattern became more squeezed, indicating the enhancement of the convection effect. The numerical study conducted for more viscose solution showed that the most symmetrical diffraction rings were observed for liquid with the highest viscosity, causing the lowest convection current. The amount of nonlinear refraction induced in the colloids was not affected by the applied ranges of thermal expansion coefficient and viscosity parameters in this study. The largest far-field diffraction pattern (beam divergence) with the most interference rings in the far-field intensity distribution for the AuNP colloids with the lowest thermal conductivity was observed. Our results show that thermo-optical properties of the colloids increase with an increase in the linear absorption coefficient of the medium, which is here attributed to the concentration of AuNPs. This simulation was completely compatible with the recorded experimental diffraction patterns using continuous laser beam at 532 nm.

REFERENCES

[١] M. Arjomandi Lari, s. parhoodeh, G. Alahverdi, and A. Rohani Sarvestani. *Investigation of optical and structural properties of iron oxide nanostructures synthesized by co-precipitation method*. Journal of Optoelectronical Nanostructures., ٧(٣) (٢٠٢٢) ١٠٨-١١٧. https://jopn.marvdasht.iau.ir/article_٥٣٣٩.html.

[٢] M. Cheraghizade. *Optoelectronic Properties of PbS Films: Effect of Carrier Gas*. Journal of Optoelectronical Nanostructures., ٤(٢) (٢٠١٩) ١-١٢. https://jopn.marvdasht.iau.ir/article_٣٤٧٤.html.

[٣] M. A. Zekavat Fetrat, M. Sabaeian, and G. Solookinejad. *The effect of ambient temperature on the linear and nonlinear optical properties of truncated pyramidal-shaped InAs/GaAs quantum dot.* Journal of Optoelectronical Nanostructures., ٦ (٣) (٢٠٢١) ٨١- ٩٢. https://jopn.marvdasht.iau.ir/article_٤٩٨٠.html .

[٤] Hossein Bahramiyan, and Somayeh Bagheri. *Linear and nonlinear optical properties of a modified Gaussian quantum dot: pressure, temperature and impurity effect.* Journal of Optoelectronical Nanostructures., ٣ (٣) (٢٠١٨) ٧٩- ١٠٠. https://jopn.marvdasht.iau.ir/article_٣٠٤٧.html.

[٥] O. bahrami, and A. Baharvand. *Nonlinear Optical Effects in One Dimensional Multi-layer Structure Consisting of Polar Ferroelectric Called LiTaO٣.* Journal of Optoelectronical Nanostructures., ٦(١) (٢٠٢١) ٢١-٣٤. https://jopn.marvdasht.iau.ir/article_٤٥٣٩.html.

[٦] M. S. Ribeiro, K. C. Ribeiro, V. M. Lenart, R. F. Turchiello, and S. L. Gómez, *PVP-Capped Gold Nanoparticles: Thermal Nonlinear Refraction Probed by Spatial Self-Phase Modulation.* physica status solidi a., ٢١٩ (٢٠٢٢) ٢١٠٠٦٠٠. https://onlinelibrary.wiley.com/doi/abs/١٠,١٠٠٢/pssa.٢٠٢١٠٠٦٠٠.

[٧] A. Akouibaa, R. Masrour, A. Jabar, M. Benhamou, M. Ouarch, and A. Derouiche. *Study of the Optical and Thermoplasmonics Properties of Gold Nanoparticle Embedded in Al٢O٣ Matrix.* Plasmonics., ١٧ (٢٠٢٢) ١١٥٧–١١٦٩. https://link.springer.com/article/١٠,١٠٠٧/s١١٤٦٨-٠٢٢-٠١٦٠٧-w.

[٨] C. Chen, K. Wang, and L. Luo. *AuNPs and ٢D functional nanomaterial-assisted SPR development for the cancer detection: a critical review.* Cancer Nanotechnology., ١٣ (٢٠٢٢) ٢٩. https://cancer-nano.biomedcentral.com/articles/١٠,١١٨٦/s١٢٦٤٥-٠٢٢-٠٠١٣٨-٧.

[٩] M. T. Pambudi et al., *Localized surface plasmon effect on ٣-mercaptopropionic acid and citrate stabilized gold nanoparticles for biosensor application.* Journal of Nonlinear Optical Physics & Materials., ٣١(٠٤) (٢٠٢٢) ٢٣٥٠٠٠٤. https://www.worldscientific.com/doi/١٠,١١٤٢/S٠٢١٨٨٦٣٥٢٣٥٠٠٠٤٢.

[١٠] L. Sarkhosh, H. Aleali, R. Karimzadeh, and N. Mansour. *Large thermally induced nonlinear refraction of gold nanoparticles stabilized by cyclohexanone.* physica status solidi (a)., ٢٠٧(١٠) (٢٠١٠) ٢٣٠٣-٢٣١٠. https://onlinelibrary.wiley.com/doi/abs/١٠,١٠٠٢/pssa.٢٠١٠٢٦٠٢١.

[١١] H. Aleali, L. Sarkhosh, M. Eslamifar, R. Karimzadeh, and N. Mansour. *Thermo-optical properties of colloids enhanced by gold nanoparticles.* Japanese Journal of Applied Physics., ٤٩(٨R) (٢٠١٠) ٠٨٥٠٠٢. https://iopscience.iop.org/article/١٠,١١٤٣/JJAP.٤٩,٠٨٥٠٠٢.

[١٢] R. F. Souza, M. A. Alencar, E. C. da Silva, M. R. Meneghetti, and J. M. Hickmann, *Nonlinear optical properties of Au nanoparticles colloidal system: local and nonlocal responses.* Applied Physics Letters., ٩٢(٢٠) (٢٠٠٨) ٢٠١٩٠٢. https://doi.org/١٠,١٠٦٣/١,٢٩٢٩٣٨٥.

[١٣] H. Aleali, L. Sarkhosh, R. Karimzadeh, and N. Mansour. *Threshold-tunable optical limiters of Au nanoparticles in castor oil.* Journal of Nonlinear Optical Physics & Materials., ٢١(٠٢) (٢٠١٢) ١٢٥٠٠٢٤. https://www.worldscientific.com/doi/abs/١٠,١١٤٢/S٠٢١٨٨٦٣٥١٢٥٠٠٢٤٥.

[١٤] L. Sarkhosh, and N. Mansour. *Study of the solution thermal conductivity effect on nonlinear refraction of colloidal gold nanoparticles.* Laser

Physics., ٢٥(٦) (٢٠١٥) ٠٦٥٤٠٤. https://iopscience.iop.org/article/١٠,١٠٨٨/١٠٥٤-٦٦٠X/٢٥/٦/٠٦٥٤٠٤.
[١٥] L. Sarkhosh, and N. Mansour. *Analysis of Z-scan measurement for large thermal nonlinear refraction in gold nanoparticle colloid*. Journal of Nonlinear Optical Physics & Materials., ٢٤(٠٢) (٢٠١٥)١٥٥٠٠١٤. https://www.worldscientific.com/doi/abs/١٠,١١٤٢/S٠٢١٨٨٦٣٥١٥٥٠٠١٤٩.
[١٦] J. Simon, S. Udayan, V. P. N. Nampoori and M. Kailasnath. *Investigations on nonlinear optical properties and thermal diffusivity of gold nanoparticle embedded protein complex*. Optics & Laser Technology., ١٣٨ (٢٠١١) ١٠٦٨٥٩. https://www.sciencedirect.com/science/article/abs/pii/S٠٠٣٠٣٩٩٢٢٠٣١٤٩٢٤.
[١٧] G. Baffou, F. Cichos, and R. Quidant. *Applications and challenges of thermoplasmonics*. Nature Materials., ١٩ (٢٠٢٠) ٩٤٦–٩٥٨. https://www.nature.com/articles/s٤١٥٦٣-٠٢٠-٠٧٤٠-٦.
[١٨] A. Kumar, A. Taneja, T. Mohanty, and R. P. Singh. *Effect of laser beam propagation through the plasmonic nanoparticles suspension*. Results in Optics., ٣ (٢٠٢١) ١٠٠٠٨١. https://www.sciencedirect.com/science/article/pii/S٢٦٦٦٩٥٠١٢١٠٠٠٢٩٨.
[١٩] B. Azemoodeh Afshar, A. Jafari, Mir M. Golzan and R. Naderali, *Nonlinear optical properties of gold nanoparticles produced by laser ablation at two different radiation wavelengths*. Results in Optics., ١٢ (٢٠٢٣) ١٠٠٤٦٢. https://www.sciencedirect.com/science/article/pii/S٢٦٦٦٩٥٠١٢٣٠٠١١٤١.
[٢٠] J. L. Domínguez-Juárez, R. Quintero-Torres, M. A. Cardoso-Duarte, M. A. Quiroz-Juárez, J. L. Aragón, and J. Villatoro. *Unveiling the properties of liquids via photothermal-induced diffraction patterns*. communications physics., ٦ (٢٠٢٣) ١٥٤. https://www.nature.com/articles/s٤٢٠٠٥-٠٢٣-٠١٢٧٨-x.
[٢١] T. Neupane, B. Tabibi, W. J. Kim, and F. J. Seo. *Spatial Self-Phase Modulation in Graphene-Oxide Monolayer*. Crystals., ١٣(٢) (٢٠٢٣) ٢٧١. https://www.mdpi.com/٢٠٧٣-٤٣٥٢/١٣/٢/٢٧١.
[٢٢] B. Pishnamazi, and E. Koushki. *Study of nonlinear optical diffraction patterns using machine learning models based on ResNet ١٥٢ architecture*. AIP Advances., ١٣(١) (٢٠٢٣) ٠١٥٠٢٠. https://pubs.aip.org/aip/adv/article/١٣/١/٠١٥٠٢٠/٢٨٧١١٦٥/Study-of-nonlinear-optical-diffraction-patterns.
[٢٣] Qusay. M. A. Hassan, C. A. Emshary, and H. A. Sultan. *Investigating the optical nonlinear properties and limiting optical of eosin methylene blue solution using a cw laser beam*. Physica Scripta., ٩٦ (٢٠٢١) ٩. https://iopscience.iop.org/article/١٠,١٠٨٨/١٤٠٢-٤٨٩٦/ac٠٨٦٨/meta.

[٢٤] Y. Shan, Z. Li, B. Ruan, J. Zhu, Y. Xiang, and X. Dai. *Two-dimensional Bi ٢S٣-based all-optical photonic devices with strong nonlinearity due to spatial self-phase modulation*. Nanophotonics., ٨(١٢) (٢٠١٩) ٢٢٢٥-٢٢٣٤. https://www.degruyter.com/document/doi/١٠,١٥١٥/nanoph-٢٠١٩-٠٢٣١/html?lang=en.

[٢٥] R. Karimzadeh. *Spatial self-phase modulation of a laser beam propagating through liquids with self-induced natural convection flow*. Journal of Optics., ١٤(٩) (٢٠١٢) ٠٩٥٧٠١. https://iopscience.iop.org/article/١٠,١٠٨٨/٢٠٤٠-٨٩٧٨/١٤/٩/٠٩٥٧٠١/meta.

[٢٦] R. Karimzadeh. *Studies of spatial self-phase modulation of the laser beam passing through the liquids*. Optics communications., ٢٨٦ (٢٠١٣) ٣٢٩-٣٣٣. https://www.sciencedirect.com/science/article/abs/pii/S٠٠٣٠٤٠١٨١٢٠٠٩٠٥٤.

[٢٧] B. M. Irivas, M. A. Carrasco, M. M. Otero, R. R. García, and M. I. Castillo. *Far-field diffraction patterns by a thin nonlinear absorptive nonlocal media*. optics Express., ٢٣(١١) (٢٠١٥) ١٤٠٣٦-١٤٠٤٣. https://opg.optica.org/oe/fulltext.cfm?uri=oe-٢٣-١١-١٤٠٣٦&id=٣١٨٩١١.

[٢٨] J. Whinnery, D. Miller, and F. Dabby. *Thermal convention and spherical aberration distortion of laser beams in low-loss liquids*. IEEE Journal of Quantum Electronics., ٣(٩) (١٩٦٧) ٣٨٢-٣٨٣. https://ieeexplore.ieee.org/abstract/document/١٠٧٤٦١٢/.

[٢٩] S. S. Sarkisov. *Circulation of fluids induced by self-acting laser beam*. Journal of applied physics., ٩٩(١١) (٢٠٠٦) ١١٤٩٠٣. https://pubs.aip.org/aip/jap/article-abstract/٩٩/١١/١١٤٩٠٣/١٤٤٠١٩/Circulation-of-fluids-induced-by-self-acting-laser?redirectedFrom=fulltext.

[٣٠] J. P. Gordon, R. C. C. Leite, R. S. Moore, S. P. S. Porto, and J. R. Whinnery, *Long-Transient Effects in Lasers with Inserted Liquid Samples*. J. Appl. Phys., ٣٦ (١٩٦٥) ٣-٨. https://pubs.aip.org/aip/jap/article-abstract/٣٦/١/٣/٣٦٥٨٥٨/Long-Transient-Effects-in-Lasers-with-Inserted?redirectedFrom=fulltext.

[٣١] Y. Shi, Y. Gao, Y. Hu, Y. Xue, and B. Gu. *Spatial self-phase modulation with tunable dynamic process and its applications in all-optical nonlinear photonic devices*. Optics and Lasers in Engineering., ١٥ (٢٠٢٢) ١٠٧١٦٨. https://www.sciencedirect.com/science/article/abs/pii/S٠١٤٣٨١٦٦٢٢٠٠٢٢١٤.

[٣٢] T. Mohamed, M. H. El-Motlak, S. Mamdouh, M. Ashour, H. Ahmed, H. Qayyum, and A. Mahmoud. *Excitation wavelenghth and colloids concentration-dependent nonlinear optical properties of silver nanoparticles synthesized by laser ablation*. Materials., ١٥ (٢٠٢٢) ٧٣٤٨. https://www.mdpi.com/١٩٩٦-١٩٤٤/١٥/٢٠/٧٣٤٨.

[٣٣] Y. Gao, Q. Chang, W. Jiao, H. Ye, Y. Li, Y. Wang, Y. Song, and D. Zhu. *Solvent dependent optical limiting behavior of lead nanowires stabilized by [٦٠] fullerene derivative*. Appl. Phys. B., ٨٨ (٢٠١٧) ٨٩–٩٢. https://link.springer.com/article/١٠,١٠٠٧/s٠٠٣٤٠-٠٠٧-٢٦٦٩-٨.

[٣٤] G. X. Chen, M. H. Hong, T. C. Chong, H. I. Elim, G. H. Ma, and W. Ji. *Preparation of carbon nanoparticles with strong optical limiting properties by laser ablation in water*. J. Appl. Phys., ٩٥ (٢٠٠٤)١٤٥٥–١٤٥٩. https://pubs.aip.org/aip/jap/article-abstract/٩٥/٣/١٤٥٥/٧٧٠٧٨٨/Preparation-of-carbon-nanoparticles-with-strong?redirectedFrom=fulltext.

[٣٥] V. Amendola, G. A. Rizzi, S. Polizzi, and M. Meneghetti. *Synthesis of gold nanoparticles by laser ablation in toluene: Quenching and recovery of the surface plasmon absorption.* J. Phys. Chem. B., ١٠٩ (٢٠١٥) ٢٣١٢٥–٢٣١٢٨. https://pubmed.ncbi.nlm.nih.gov/١٦٣٧٥٢٧١/.

[٣٦] M. Sheik-Bahae, A. A. Said, T. H. Wei, D. J. Hagan, and E. W. Van Stryland. *Sensitive measurement of optical nonlinearities using a single beam*. IEEE journal of quantum electronics., ٢٦(٤) (١٩٩٠) ٧٦٠-٧٦٩. https://ieeexplore.ieee.org/document/٥٣٣٩٤.

[٣٧] A. A. Said, M. Sheik-Bahae, D. J. Hagan, T. H. Wei, J. Wang, J. Young, and E. W. Van Stryland. *Determination of bound-electronic and free-carrier nonlinearities in ZnSe, GaAs, CdTe, and ZnTe*. JOSA B., ٩(٣) (١٩٩٢) ٤٠٥-٤١٤. https://opg.optica.org/viewmedia.cfm?r=١&rwjcode=josab&uri=josab-٩-٣-٤٠٥&html=true.

[٣٨] L. Agiotis, and M. Meunier. *Nonlinear thermal lensing of high repetition rate ultrafast laser light in plasmonic nano-colloid*. Nanophotonics., ١١(٥) (٢٠٢٢) ١٠٥١–١٠٦٢. https://www.degruyter.com/document/doi/١٠,١٥١٥/nanoph-٢٠٢١-٠٧٧٥/html?lang=en.

[٣٩] Yu-Chien Huang, Te-Hsin Chen, Jz-Yuan Juo, Shi-Wei Chu, and Chia-Lung Hsieh. *Quantitative Imaging of Single Light-Absorbing Nanoparticles by Widefield Interferometric Photothermal Microscopy*. ACS Photonics., ٨ (٢٠٢١) ٥٩٢–٦٠٢. https://pubs.acs.org/doi/abs/١٠,١٠٢١/acsphotonics.٠c٠١٦٤٨.

[٤٠] Yi-Shiou Duh, Y. Nagasaki, Yu-Lung Tang, Pang-Han Wu, Hao-Yu Cheng, Te-Hsin Yen, Hou-Xian Ding, K. Nishida, I. Hotta, Jhen-Hong Yang, Yu-Ping Lo, Kuo-Ping Chen, K. Fujita, Chih-Wei Chang, Kung-Hsuan Lin, J. Takahara, and Shi-Wei Chu. *Giant photothermal nonlinearity in a single silicon nanostructure*. Nature Communications., ١١ (٢٠٢٠) ٤١٠١. https://www.nature.com/articles/s٤١٤٦٧-٠٢٠-١٧٨٤٦-٦.

[٤١] R. Karimzadeh, and M. Arshadi. *Thermal lens measurement of the nonlinear phase shift and convection velocity*. Laser Phys., ٢٣ (٢٠١٣) ١١٥٤٠٢. https://iopscience.iop.org/article/١٠,١٠٨٨/١٠٥٤-٦٦٠X/٢٣/١١/١١٥٤٠٢/meta.

[٤٢] H. Aleali, and N. Mansour. *Thermal-induced nonlinearity enhancement in Ag nanoparticles colloids by low thermal conductivity liquids*. Journal of Optics., ٤٨(٢) (٢٠١٩) ١٧٢-١٧٨. https://link.springer.com/article/١٠,١٠٠٧/s١٢٥٩٦-٠١٩-٠٠٥٢٠-٦.

[٤٣] S. Hashemi Zadeh, M. Rashidi-Huyeh, and B. Palpant. *Enhancement of the thermo-optical response of silver nanoparticles due to surface plasmon resonance.* Journal of Applied Physics., ١٢٢(١٦) (٢٠١٧) ١٦٣١٠٨. https://ui.adsabs.harvard.edu/abs/٢٠١٧JAP...١٢٢p٣١٠٨H/abstract.